T-box transcription factor 15 regulated by methyltransferase-like 3-mediated N6-methyladenosine modification promotes immune escape and progression of gastric cancer by activating matrix metalloproteinase 14 transcription

HONGSAI HU[1], RONG HE[1], MINJI LIU[1], XULI LIU[1], QIONGJIA AI[1], MIN CHEN[1], QIAN WANG[1], WENHUI CHEN[2] and WEIMING QU[1]

[1]Department of Gastroenterology, Medical Center of Digestive Disease, Zhuzhou Hospital Affiliated to Xiangya School of Medicine, Central South University, Zhuzhou, Hunan 412007, P.R. China; [2]Zhuzhou Clinical College, Jishou University, Jishou, Hunan 416000, P.R. China

Received December 25, 2025; Accepted June 15, 2026

DOI: 10.3892/ijo.2026.5913

Abstract. The present study aimed to investigate the involvement of T-box transcription factor 15 (TBX15) in the immune evasion by gastric cancer (GC) cells, as well as the molecular pathways that regulate TBX15 upstream and downstream. GC and paracancerous tissues were collected to verify the expression of TBX15, matrix metalloproteinase 14 (MMP14) and methyltransferase-like 3 (METTL3) using reverse transcription-quantitative PCR and western blotting. The co-culture system of GC cell-tumor-associated macrophages (TAMs) and mouse forestomach carcinoma (MFC) cell-CD8$^+$ T cells was constructed. TBX15, MMP14 and METTL3 were highly expressed in GC tissues. Kaplan-Meier analyses were performed, and high *TBX15* expression predicted a poor prognosis for patients with GC. Silencing *TBX15* promoted GC cell apoptosis and inhibited tumor development and the activity of proliferation, migration and invasion. TBX15 targeted the *MMP14* promoter by using ChIP-qPCR. Overexpression of *MMP14* attenuated the reduction caused by *TBX15* silencing. METTL3 targets *TBX15* mRNA and regulates the m6A level of *TBX15*. TBX15 is associated with macrophage and CD8$^+$ T cell infiltration. In the co-culture system of GC-TAM and MFC-CD8$^+$ T cells, *TBX15* overexpression alleviated the decrease in M2 polarization and activation of CD8$^+$ T cell antitumor activity caused by *METTL3* silencing. However, *MMP14* overexpression resulted in *TBX15* silence-induced decreases in M1 macrophage polarization and CD8$^+$ T cell activity. These data suggested that TBX15, correlated with poor prognosis in patients with GC, promotes immune escape in GC cells. TBX15, regulated by m6A methylation, targeted the MMP14 promoter, thereby regulating MMP14 expression. The METTL3/TBX15/MMP14 signaling axis was involved in GC cell development, M2 macrophage polarization and CD8$^+$ T cell antitumor activity activation. These findings provide a fundamental experimental rationale for TBX15 as a potential therapeutic target for GC.

Correspondence to: Dr Weiming Qu, Department of Gastroenterology, Medical Center of Digestive Disease, Zhuzhou Hospital Affiliated to Xiangya School of Medicine, Central South University, 116 Changjiang South Road, Zhuzhou, Hunan 412007, P.R. China
E-mail: qwmq2q2@163.com

Key words: T-box transcription factor 15, gastric cancer, m6A, macrophages, CD8$^+$ T cell

Introduction

Gastric cancer (GC) is one of the most common malignant tumors in the world with a high incidence (5.6% of all cancers) (1,2). Genetic susceptibility is one of the important risk factors for GC (3-5). Germline mutations in the E-cadherin gene (CDH1) or microsatellite instability in the DNA mismatch repair gene hMLH1 are associated with familial GC (6,7). In addition to genetic factors, the risk factors for GC are also associated with *Helicobacter pylori* infection and unhealthy lifestyles, including alcohol consumption, high-salt diet and smoking (2,8). Due to the lack of clear clinical indications, most patients were in the advanced stage of GC at diagnosis, accompanied by poor prognosis (1,9). The innovation of molecular analysis technology has improved the efficiency and accuracy of prediction of diagnostic and targeted therapy markers (10). The diversification of treatment methods such as chemotherapy, targeted therapy, and immunotherapy and the innovation of molecular diagnostic technology have prolonged the survival of patients, but the 5-year survival of patients with GC is still less than 30% (9,11). Therefore, it is essential to find effective early markers for the diagnosis and treatment of GC.

T-box transcription factor 15 (TBX15) belongs to the T-box gene family, encoding a phylogenetically conserved transcription factor family. Members of this family have a highly conserved characteristic sequence of 180 amino acid residues

that can bind to DNA, and their target genes contain one or more T half-sites in the upstream promoter sequence (12,13). TBX15 has been found to play a role in the regulation of various diseases, such as heart failure (14), osteoporosis (15), obesity (16) and cancer development (17,18). In multiple tumor studies, TBX15 was associated with poor prognosis in patients with glioma (18,19) and colorectal cancer (20). In addition, TBX15 enriched in glioma was associated with immunosuppressive genes (19). It can be hypothesized that TBX15 may participate in the immune escape process of cancer cells. In a GC study, TBX15 was implicated in GC cell proliferation and drug antitumor pathways (21). However, the regulatory pathways of TBX15 related to the prognosis of patients with GC and their immune escape remain an unsolved problem.

N6-methyladenosine (m6A) is a kind of RNA modification, which widely exists in eukaryotic mRNA modification. The m6A WERs ('writers', 'erasers' and 'readers') control the dynamic modification process of m6A, which is mainly regulated by proteins methyltransferase-like 3 (METTL3), methyltransferase 14 (METTL14), YTH-domain-containing proteins (YTHDFs), insulin-like growth factor 2 mRNA-binding proteins (IGF2BPs) and demethylases (FTO and ALKBH5) (22). m6A methylation affects the physiological process of cells by regulating the fate of downstream mRNAs. These include maintenance of RNA stability (23-25), mRNA nuclear export (26,27) and microRNA processing (28). The effect on RNA stability is mainly achieved by m6A 'reader' proteins that are connected to downstream molecular pathways. In the cytoplasm, the YTHDF protein family is able to preferentially recognize m6A-containing RNAs and subsequently direct them to degradation pathways (29). A key member of the m6A methyltransferase complex is METTL3, which acts as a reversible epitranscriptomic regulator. During m6A modification, METTL3 acts as an enzyme responsible for catalyzing m6A deposition and forms a complex with several other proteins that act together to promote m6A deposition on RNA (30,31). m6A modification plays a role in the development of various types of cancer (32,33). In multiple cancer studies, METTL3 has been linked to the malignant advancement of tumors and poor prognosis of patients, including colorectal cancer (34), cervical cancer (35), hepatocellular carcinoma (36) and GC (37). Its regulatory mechanisms include glycolysis, self-renewal, tumorigenicity and metastasis of tumor cells. However, the specific molecular mechanisms through which METTL3 is involved in immune escape in GC cells remain unclear.

The present study aims to investigate the role of TBX15 in mediating immune escape of GC cells, analyze and determine the regulatory relationship between *TBX15* mRNA and m6A methylation modification, so as to enhance the understanding of TBX15 in GC cell immune escape and provide new ideas for future GC-targeted therapy.

Materials and methods

Materials. The human gastric mucosal epithelial cell (GES-1; cat. no. AW-CNH199), human GC cell lines HGC27 (cat. no. AW-CNH127) and MKN74 (cat. no. AW-CCH277), mouse forestomach carcinoma (MFC; cat. no. AW-CCM404) and tohoku hospital pediatrics-1 (THP-1; AW-CCH098) were purchased from Abiowell (https://www.abiowell.com/). All plasmids were purchased from Honor Gene Co., Ltd. These included *TBX15* silencing (si-*TBX15*; cat. no. HG-SH152380), *TBX15* overexpression (oe-*TBX15*; cat. no. HG-HO152380), matrix metalloproteinase 14 (MMP14) overexpression (oe-*MMP14*; cat. no. HG-HO004995), *METTL3* silencing (si-*METTL3*#1-3; cat. no. HG-SH019852), *MMP14*-wt (cat. no. HG-YO020961) and *MMP14*-mut (cat. no. HG-YO020961M). Male C57BL/6 mice (6 weeks) were ordered from Hunan SJA Laboratory Animal Co., Ltd. TRIzol (Thermo Fisher Scientific, Inc.), mRNA reverse transcription kit (CWBIO), and UltraSYBR Mixture (CWBIO) were used for reverse transcription-quantitative PCR (RT-qPCR) analysis. 5-Ethynyl-2'-deoxyuridine (EdU) kit (cat. no. C10310) was purchased from Guangzhou RiboBio Co., Ltd. Annexin V-APC assay kit (Nanjing KeyGen Biotech Co., Ltd.) and TUNEL assay kit (cat. no. 40306ES50; Yeasen Biotechnology) (https://www.yeasen.com/) were used to detecT cell death. The inducible nitric oxide synthase (iNOS; cat. no. CSB-E08326m), IL-1β (cat. no. CSB-E08054m), TNF-α (cat. no. CSB-E04741m), Arg-1 (cat. no. CSB-EL002005MO), IL-10 (cat. no. CSB-E04594m) and CD206 (cat. no. CSB-EL014782MO) kits were purchased from Wuhan Huamei Biotech Co., Ltd. The m6A assay kit (cat. no. P-9005; EpiGentek) was used to analyze m6A detection. MeRIP-qPCR kit (cat. no. 17-700) and Actinomycin D (cat. no. A4262) were purchased from MilliporeSigma. A dual luciferase assay kit (cat. no. E1910) was purchased from Promega Corporation. All antibody information is shown in Table SI.

Data acquisition and bioinformatics analysis. The RNA sequencing profiles and clinical data for 33 cancerous from the Cancer Genome Atlas (TCGA, https://portal.gdc.cancer.gov/) and Genotype-Tissue Expression (GTEx) cohorts (GTEx Analysis Release V8, https://gtexportal.org) were retrieved from the University of California Santa Cruz Xena database (https://xenabrowser.net/datapages/). Univariate Cox regression (uniCox) and Kaplan-Meier analyses were performed. The R packages 'survminer' and 'survival' visualized the results, including overall survival (OS), disease-specific survival (DSS), disease-free interval (DFI) and progression-free interval (PFI) of patients with GC. JASPAR online software (https://jaspar.elixir.no/) was used to predict potential downstream targets of transcription factors. SRAMP online software (http://www.cuilab.cn/sramp) predicted m6A modification sites on RNA. RM2Target (http://rm2target.canceromics.org/#/home) predicted m6A-associated enzymes that bind to target genes.

Collection and processing of clinical samples. GC tissue samples (n=10) and corresponding paracancerous tissue samples were collected. All samples were obtained from patients with GC in Zhuzhou Hospital Affiliated to Xiangya School of Medicine, Central South University between May 2024 and May 2025. The procedures followed in the present study were approved (approval no. ZZCHEC2022070-01) by the Ethics Committee (Zhuzhou, China) and performed followed Declaration of Helsinki Guideline. Written informed consent was obtained from each enrolled subject. The baseline information statistics of patients are shown in Table SII.

Cell culture and treatments. Cells were cultured in RPMI-1640 containing 10% fetal bovine serum (both from Gibco; Thermo Fisher Scientific, Inc.) and 1% penicillin/streptomycin. The cell incubator environment was maintained at 37˚C with a humidified atmosphere containing 5% CO_2.

To explore the effects of TBX15, MMP14 and METTL3 on GC cells, plasmid intervention experiments of si-*TBX15*, oe-*TBX15*, oe-*MMP14* and si-*METTL3*#1-3 were performed. The corresponding plasmids and negative control (si-NC and oe-NC) were transfected into cells. si-*TBX15*#1-3 sequences are as follows: si-*TBX15*#1, 5'-GACAATAAAAGATACAGATAT-3'; si-*TBX15*#2, 5'-GGGGTGAAAACGTTCAACTTT-3'; si-*TBX15*#3, 5'-GACATATACCCAAGAACAAGA-3'. si-*METTL3*#1-3 sequences are as follows: si-*METTL3*#1, 5'-GAGTTGATTGAGGTAAGCGA-3'; si-*METTL3*#2, 5'-TAGAGCTATTAAATACTACAA-3'; si-*METTL3*#3, 5'-GACGAATTATCAATAAACACA-3'. si-NC sequence is 5'-TGCGGGGCTAGGGTCCAACGG-3'.

A co-culture system of GC cell-TAM cells was constructed. The THP-1 was resuspended in RPMI-1640 medium and seeded in 6-well culture plates at a density of $7.5x10^5$ cells/well. THP-1 cells were treated with phorbol 12-myristate 13-acetate (PMA; 320 nmol/l) for 6 h and then co-cultured with tumor cells for 24 h. After washing the cells with PBS, they were resuspended in serum-free RPMI-1640 medium. Macrophages were harvested, and flow analysis was performed.

A co-culture system of MFC cell-$CD8^+$ T cells was established. Spleen-derived $CD8^+$ T cells were isolated using MojoSort™ Mouse $CD8^+$ T cell Isolation kit (BioLegend, Inc.). Isolated $CD8^+$ T cells were activated with Ultra-LEAF™ purified anti-mouse CD3/CD28 (BioLegend, Inc.) for 3 days following the manufacturer's protocol. IL-2 (10 ng/ml) was added to RPMI-1640 medium for experiments. Transfected MFC cells were co-incubated with activated $CD8^+$ T cells for 48 h. The ratio of tumor cells to $CD8^+$ T cells was 1:1-1:20. $CD8^+$ T cells were collected and analyzed for granzyme B (GZMB), perforin (PFP), CD100, IFN-γ and TNF-α expression.

Animals. A total of 48 C57BL/6 mice (male, 6 weeks old, ~20 g) were maintained under pathogen-free conditions for 1 week. Mice were raised on a 12 h/12 h light/dark cycle (22~25˚C) with *ad libitum* access to water and food. All animal experiments were conducted in accordance with animal care, animal welfare and ethics. It has been approved by the Institutional Animal Care and Use Committee (IACUC) of the Second Xiangya Hospital, Central South University (approval no. 2022722).

Experiment 1: Mice were randomly divided into 3 groups (n=6): Control group, sh-NC group and sh-*TBX15* group. Mice in the sh-NC and sh-*TBX15* groups were injected with $1x10^6$ MFC cells (100 μl, resuspended in PBS) that had been transfected with sh-NC and sh-*TBX15* plasmids. At room temperature, 3 μg of sh-NC and sh-TBX15 plasmids were transfected into MFC cells by using Lipofectamine™ 2000 (Invitrogen; Thermo Fisher Scientific, Inc.). At 48 h after transfection, cells were collected immediately for injection. The injection site was the right underarm. MFC cells injected in the Control group were not treated. The body weight and tumor were observed twice a week, and the tumor volume was measured with vernier calipers. The tumor volume was calculated by the formula $V=(L \times W^2)/2$, where V was the volume (mm^3), L was the maximum diameter (mm), and W was the minimum diameter (mm). The experiment was finished 21 days after tumor seeding, and animals were euthanized by intraperitoneal injection of 200 mg/kg sodium pentobarbital solution. Samples were received and images were captured after euthanasia. sh-*TBX15* sequence is 5'-GACAATAAAAGATACAGATAT-3' and sh-NC sequence is 5'-TGCGGGGCTAGGGTCCAACGG-3'.

Experiment 2: Mice were randomly divided into 5 groups (n=6): Control group, sh-NC group, sh-*METTL3* group, sh-*METTL3* + oe-NC group, sh-*METTL3* + oe-*TBX15* group. Consistent with the aforementioned intervention procedure, MFC cells subjected to sh-METTL3 and oe-*TBX15* interventions were injected into the right armpit of mice. After 21 days, mice were euthanized by intraperitoneal injection of sodium pentobarbital solution (200 mg/kg) and tumors were collected. sh-*METTL3* sequence is 5'-GACGAATTATCAATAAACACA-3'. sh-NC sequence is 5'-TGCGGGGCTAGGGTCCAACGG-3'.

RT-qPCR analysis. To detect gene expression in tissues and cells, qPCR analysis was performed (38). Total RNA was extracted from GC tissues, mouse tumor bodies, and cells using TRIzol reagent, and the concentration was determined by ultraviolet spectrophotometer. cDNA was synthesized using an mRNA reverse transcription kit according to the manufacturer's instructions. qPCR was applied to detect the mRNA levels using UltraSYBR Mixture. PCR reaction conditions were 95˚C for 10 min, and 95˚C for 15 sec, and 60˚C for 30 sec, for 40 cycles. Melting curve analysis was performed with a temperature gradient of 60-95˚C. The primers were designed by primer5 (https://premierbiosoft.com/) and synthesized by the TsingKe Biological Technology. The relative mRNA levels of the target genes were determined by the $2^{-\Delta\Delta Cq}$ method (39) and normalized to β-actin (as an endogenous control). All primer sequences are included in Table SIII.

Western blotting. To determine the protein levels of TBX15, MMP14, Granzyme B, Perforin, CD100, IFN-γ, TNF-α and METTL3, western blotting was performed. Referring to a previous study (40), total protein was extracted from GC tissues and cells using the RIPA lysis buffer (Beyotime Institute of Biotechnology). A BCA assay kit was performed to detect protein concentrations. Equal amounts of protein (15-20 μg) were separated on a 10% SDS-PAGE gel and then transferred to a nitrocellulose membrane. After 5% skim milk was used for incubation and blocking for 90 min at room temperature, freshly prepared specific primary antibodies were used to incubate the membranes at 4˚C overnight. After incubation with the secondary antibody (90 min, room temperature) was completed, ECL chemiluminescence solution was added to the membrane, followed by imaging using a gel imaging system (ChemiScope6100, Clinx). β-actin was applied to normalize the target protein levels. Relative expression level of the target protein=gray value of target protein/gray value of internal reference (β-actin).

Immunohistochemistry (IHC) analysis. After the mouse tumor and GC tissues were fixed in paraffin for 24 h at

room temperature, the samples were sectioned (2 μm) (25). After deparaffinization with xylene, it was then rehydrated with graded ethanol series. The sections were immersed in 0.01 M sodium citrate antigen repair solution (pH 6.0) and heated in a microwave oven for thermal antigen repair. Incubation with 1% periodate for 15 min was used to inactivate endogenous enzymes. After incubation with specific primary antibodies (4˚C overnight) anti-TBX15, anti-Ki67, anti-PD-L1, anti-CD100, anti-IFN-γ and anti-TNF-α, sections were subjected to secondary antibody incubation for 30 min at 37˚C. After DAB color development, hematoxylin counterstain was performed, after which section images were randomly acquired. Data are presented as the mean IOD and positive rate. Positive rate was calculated as follows: (Number of positive cells/the number of total cells) x100%.

Cell proliferation assays. To detect the proliferative activity of GC cells, Cell Counting Kit-8 (CCK-8) assay (Dojindo Laboratories, Inc.) and 5-Ethynyl-2'-deoxyuridine (EdU) analysis were performed. For CCK-8 assay, 10 μl CCK-8 reagent was added to prepared cells ($5x10^3$ cells) and incubated for 4 h at 37˚C, followed by detection of absorbance values (OD values) in each well at 480 nm.

The EdU cell proliferation kit was performed. Cells were seeded into a culture medium containing EdU reagent and incubated overnight. Cells were fixed by incubation with 4% paraformaldehyde for 30 min at room temperature. After incubation with 100 μl of 1X Apollo® reaction solution for staining, 1X Hoechst33342 reaction solution was added for staining (30 min at room temperature). Images were captured using a fluorescence microscope. Cell proliferation rate was calculated as follows: (Number of Edu-positive cells/total number of cells) x100%.

Flow cytometry (FCM). To analyze the level of apoptosis, an Annexin V-APC assay kit was performed (25). Prepared cells were harvested. The Annexin V-APC and Propidium Iodide reagents were added. Reaction was performed at room temperature and in the dark for 10 min before analysis using flow cytometry (CytoFLEX; Beckman Coulter, Inc.). Data were analyzed with the use of CytExpert software (version 2.5; Beckman Coulter, Inc.). Apoptotic rate (%) was calculated as follows: Early apoptotic rate (%) + late apoptotic rate (%).

To analyze the polarization of M1 and M2 macrophages, CD86 and CD206 positive cells were identified using flow cytometry. After digestion and washing of the cells, anti-CD86 or anti-CD206 antibodies were added. FCM was used for analysis after 30 min of staining in the dark. Percentage of positive cells (%) was calculated as follows: (Cells expressing a marker/targeT cell population) x100%.

Wound healing assay. GC cells were seeded in 6-well culture plates until a monolayer was formed. A micropipette tip (200 μl) was used to generate the wound. Sterile PBS was used to wash and remove suspended cells. Image of the scratch was captured at 0 h. After incubation in serum-free Dulbecco's Modified Eagle Medium (DMEM) medium for 24 and 48 h, images were captured again for recording. A total of 3 visual fields were taken at each time point.

Invasion assays. Cell invasion ability was determined by performing Transwell assays (41) with 8-μm-pore membranes. Stably transfected GC cells ($2x10^6$ cells/well) were seeded into the upper chamber, and 10% fetal bovine serum culture medium was added to the lower chamber. After culturing at 37˚C for 48 h, cells on the upper surface of the filter were removed by wiping with a cotton ball. Next, the filter was fixed with 4% paraformaldehyde for 20 min and stained with 0.1% crystal violet for 5 min at room temperature. A total of three randomly selected fields were counted under a light microscope.

TUNEL staining. To detect apoptosis in the tumor tissue, TUNEL staining was performed using a TUNEL assay kit according to the manufacturer's instructions. DAPI working solution (5 μg/ml) was used to stain the nuclei. A fluorescence microscope was used to view the images. A total of 6 fields of view were randomly selected for assessment. Data are presented in the form of positive rates. Positive rate was calculated as follows: (Number of positive cells/the number of total cells) x100%.

Measurement of iNOS, IL-1β, TNF-α, Arg-1, IL-10 and CD206 levels. After total protein extraction from mouse tumor bodies, the levels of iNOS, IL-1β, TNF-α, Arg-1, IL-10 and CD206 were measured by commercial kits according to the manufacturer's instructions. An absorbance (OD) value at 450 nm was used to quantify protein levels. Final sample concentration equals measured concentration/protein concentration.

Dual-luciferase reporter assay. A dual luciferase assay kit was used to detect targeting between TBX15 and MMP14 according to manufacturer's instructions. The *MMP14*-wt, *MMP14*-mut and *TBX15* overexpression plasmid were transiently transfected into cells using Lipofectamine™ 2000 (Invitrogen; Thermo Fisher Scientific, Inc.). A reference reporter plasmid containing *Renilla* luciferase (pRL-TK) was co-transfected into the cells to regulate the transfection efficiency. After 48 h, cells were harvested and lysed for 15 min. Cell lysates were obtained for analysis of luciferase activity. The *MMP14*-mut sequence is: 5'-ACCACACT-3'.

ChIP-qPCR. ChIP-qPCR was performed to analyze the targeting relationship between TBX15 and *MMP14* promoters. Immunoprecipitation was performed using anti-TBX15 and IgG. qPCR was performed to quantify the immunoprecipitated DNA. The primers used for ChIP-qPCR are shown in Table SI.

Detection of m6A methylation levels. The m6A assay kit was performed to detect the global m6A levels. The cells and tissues were harvested and total RNA was extracted. The working solution of anti-m6A was used to incubate the samples for 30 min. The reaction was performed with the developer solution at room temperature in the dark for 10 min. After the terminator stop solution for 10 min, the m6A level was quantified by observing the absorbance value (OD values) at 450 nm. m6A (ng)=[Sample OD -NC OD)/Slope, m6A %=(m6A Amount (ng)]/S x100%. Slope is the slope of the standard curve, and S is the amount of input sample RNA in ng (200 ng).

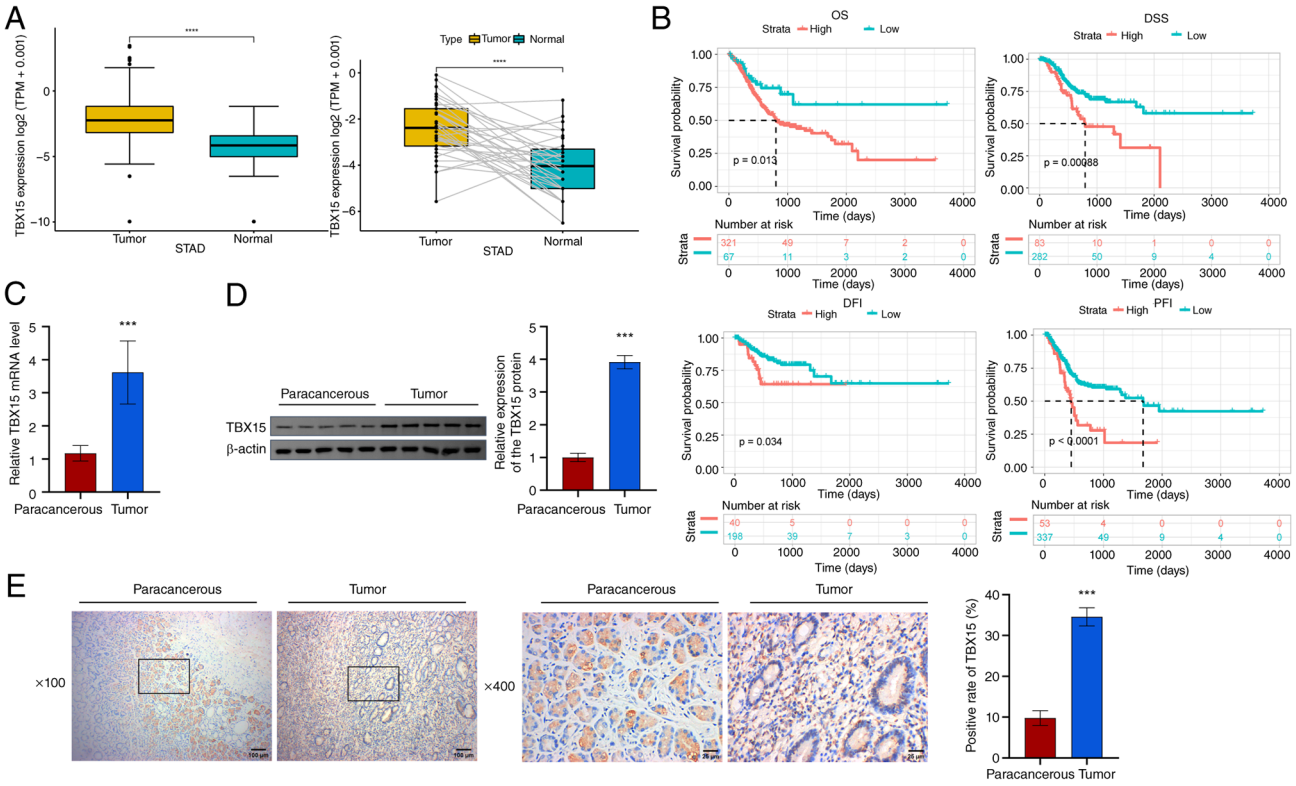

Figure 1. *TBX15* is associated with poor prognosis of patients with GC. (A) *TBX15* expression in The Cancer Genome Atlas-STAD data (unpaired and paired samples). ****P<0.0001. (B) Survival analysis of patients with GC with high and low *TBX15*. (C-E) TBX15 levels. Scale bars, 100 and 25 μm. ***P<0.001 vs. paracancerous, two-tailed t-test. TBX15, T-box transcription factor 15; STAD, stomach adenocarcinoma; GC, gastric cancer.

MeRIP-qPCR. A MeRIP-qPCR kit was applied to detect the m6A levels of the target genes (25). Total RNA was extracted from GC cells. Samples were coupled to protein A/G magnetic beads (40 μl) overnight in IP buffer containing anti-m6A and anti-IgG. m6A-modified *TBX15* was enriched. qPCR was performed to detect *TBX15* levels with m6A modification.

RNA pull-down assays. METTL3 and *TBX15* mRNA binding was identified. The prepared cells were harvested and total protein was extracted. The *TBX15* mRNA probe, which was used as a bait factor, was bound to streptavidin magnetic beads. Total protein was mixed with magnetic beads after probe binding and incubated for 60 min. After elution, proteins were collected and assayed for METTL3 protein expression.

RNA stability assay. GC cells were cultured in a culture medium containing Actinomycin D (5 μg/ml) for specific periods of time (42). Cells were collected for total RNA extraction. The stability of *TBX15* mRNA was analyzed by measuring the mRNA level of *TBX15* by qPCR.

Statistical analysis. All experimental data were presented as the mean ± standard deviation (SD). GraphPad Prism (version 9.0.0; Dotmatics) was employed to perform data analysis. The Shapiro-Wilk test was employed to analyze the normality of the data. The two-tailed t-test (data comparison between two groups), one-way ANOVA, and two-way ANOVA (data comparison between multiple groups) were applied. Post hoc tests for multiple group comparisons were performed using Tukey's multiple comparisons test. P<0.05 was considered to indicate a statistically significant for comparison between groups.

Results

Prognosis-related TBX15 is highly expressed in GC. Based on TCGA and GTEx pan-cancer data, *TBX15* expression was analyzed. *TBX15* was enriched in cancer tissues in 21 tumors, including GC (TCGA-STAD) (Fig. S1A). In TCGA-STAD, *TBX15* was significantly highly expressed in both unpaired and paired GC samples (Fig. 1A). Pan-cancer prognostic data for *TBX15* is presented in Fig. S1B. *TBX15* was a high-risk factor for GC (TCGA-STAD) in OS, DSS and PFI analyses (OS, P=0.048; DSS, P=0.007; PFI, P=0.003). Patients with GC with high *TBX15* predicted shorter survival time (OS, P=0.013; DSS, P=0.00088; DFI, P=0.034; PFI, P<0.0001; Fig. 1B). Next, the TBX15 levels were analyzed in the collected GC tissues [*TBX15* mRNA: 3.62±0.95; TBX15 (1G): 3.92±0.20; TBX15 (1H): 34.58±2.22] and their paracancerous tissues [*TBX15* mRNA: 1.18±0.23; TBX15 (1D): 1.00±0.13; TBX15 (1E): 9.80±1.80] (Fig. 1C-E). TBX15 was highly expressed in GC. The aforementioned results proved that TBX15, which is associated with poor prognosis in patients with GC, was enriched in GC.

Knockdown of TBX15 inhibits the proliferation, migration and invasion of GC cells. To further explore the involvement of TBX15 in GC cells, the expression of TBX15 was identified in GC cells (HGC27 and MKN74). GES-1 (*TBX15* mRNA: 1.00±0.05; TBX15: 0.09±0.01) was used as control. TBX15

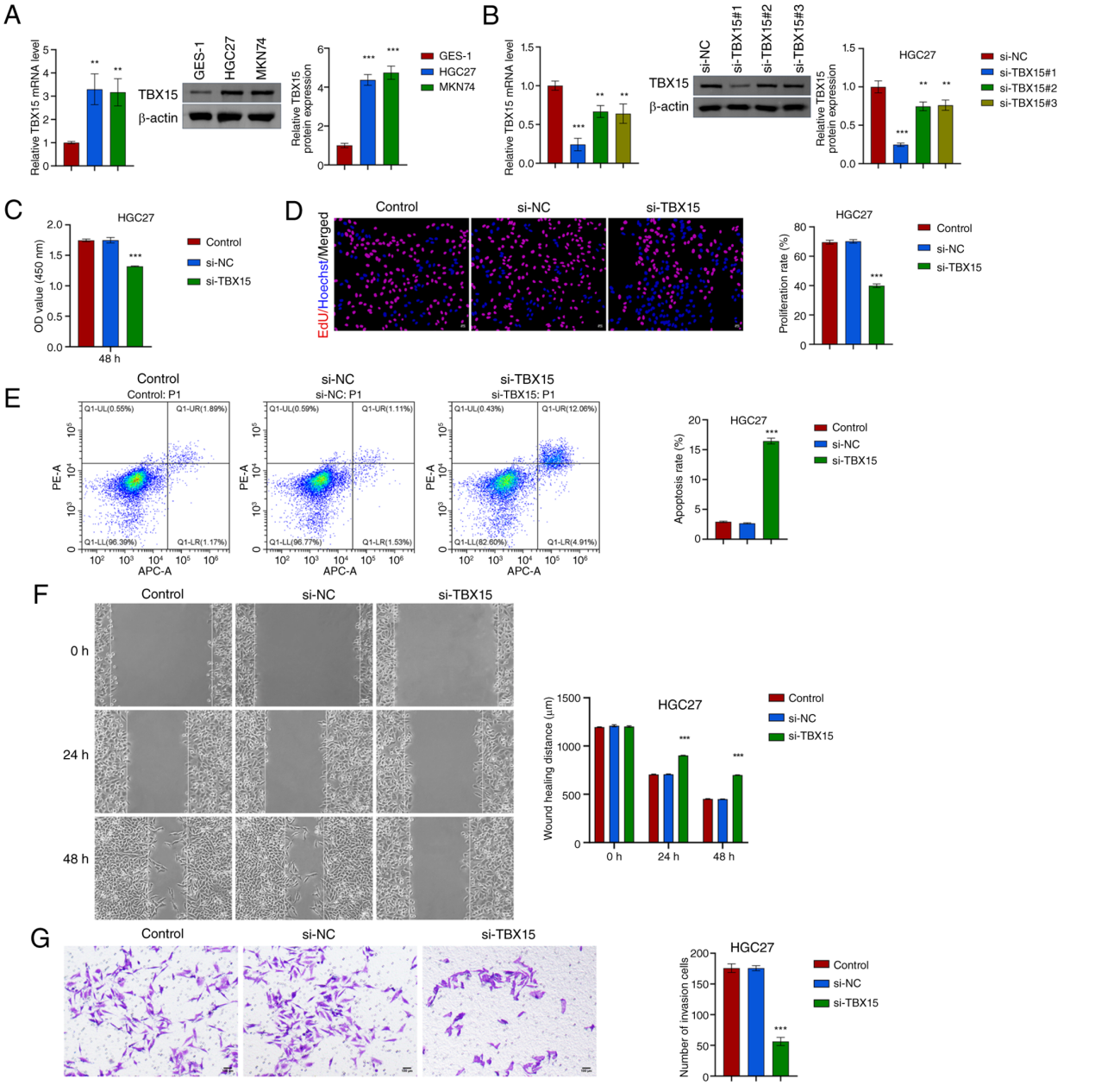

Figure 2. Silencing *TBX15* inhibits the proliferation, migration and invasion of HGC27 cells. (A) In GES-1 and GC cells (HGC27 and MKN74), TBX15 expression was verified. **P<0.01 and ***P<0.001 vs. GES-1, one-way ANOVA. (B) *TBX15* mRNA and protein levels were detected after silencing *TBX15* in HGC27. (C) Cell Counting Kit-8 assay. (D) EdU analysis. Scale bar, 50 μm. (E) Flow cytometric analysis of GC cell apoptosis levels. (F) Wound healing analysis. Scale bar, 100 μm. (G) Transwell assay was used to analyze cell invasion ability. Scale bar, 100 μm. ***P<0.001 vs. si-NC, one-way ANOVA and two-way ANOVA. TBX15, T-box transcription factor 15; GC, gastric cancer; si-, small interfering; NC, negative control.

was highly expressed in HGC27 (*TBX15* mRNA: 3.30±0.67; TBX15: 0.39±0.03) and MKN74 (*TBX15* mRNA: 3.17±0.58; TBX15: 0.43±0.03) cells (Fig. 2A). The *TBX15*-silenced cells were successfully constructed in HGC27 and MKN74 (Figs. 2B and S2A). Proliferation ability decreased after silencing *TBX15* (Fig. 2C and D; Fig. S2B and C). *TBX15* silencing promoted GC cell apoptosis (Figs. 2E and S2D). The effect of *TBX15* silencing intervention on GC cell migration was analyzed. At 24 and 48 h, the cell migration distance in the si-*TBX15* group (HGC27: 934.1±253.1; MKN74: 934.1±177.2) was lower than the si-NC group (HGC27: 788.8±386.5; MKN74: 836.4±251.8) (Figs. 2F and S2E). Transwell was performed to analyze the invasion ability of GC cells. *TBX15* silencing inhibited cell invasion (Figs. 2G and S2F). These data proved that knockdown of *TBX15*, which is highly expressed in HGC27 and MKN74, inhibited the proliferation, migration and invasion of GC cells.

Knockdown of TBX15 inhibits the tumorigenic ability of MFC cells in mice. Next, the effect of TBX15 on GC development was analyzed by tumor burden. MFC cells with or without sh-*TBX15* intervention were subcutaneously injected into mice to induce tumor formation. The tumor volume (maximum diameter: 14.78 mm, maximum volume: 1181.46 mm^3) and weight decreased after *TBX15* silencing (Fig. 3A-C). *TBX15* silencing reduced tumor burden in mice. The apoptotic rate

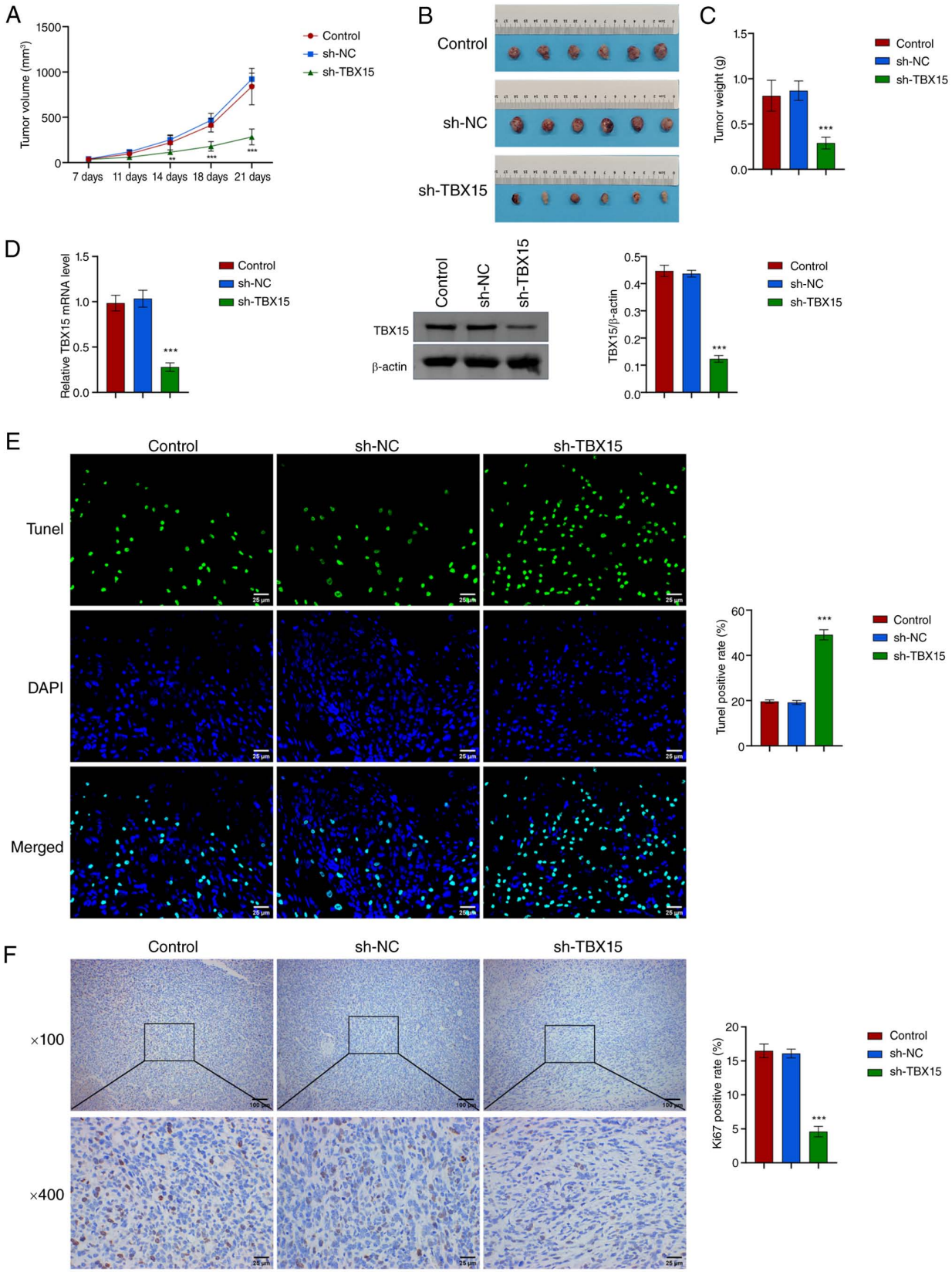

Figure 3. *TBX15* silencing inhibits GC development. (A) Tumor growth curve. (B) View of the tumor. (C) Tumor weight. (D) Expression of TBX15. (E) TUNEL staining analysis. Scale bar, 25 μm. (F) Immunohistochemistry was used to analyze Ki67 expression. Scale bars, 100 and 25 μm. **P<0.01 and ***P<0.001 vs. sh-NC, one-way ANOVA and two-way ANOVA. TBX15, T-box transcription factor 15; sh-, short hairpin; NC, negative control; GC, gastric cancer.

increased, and Ki67 levels decreased (Fig. 3D-F). These evidence demonstrated that *TBX15* silencing could inhibit GC development *in vivo*.

TBX15 regulates MMP14 transcription by binding to the MMP14 promoter. MMP14 is a membrane-anchored matrix metalloproteinase. Based on the patient data in TCGA-STAD,

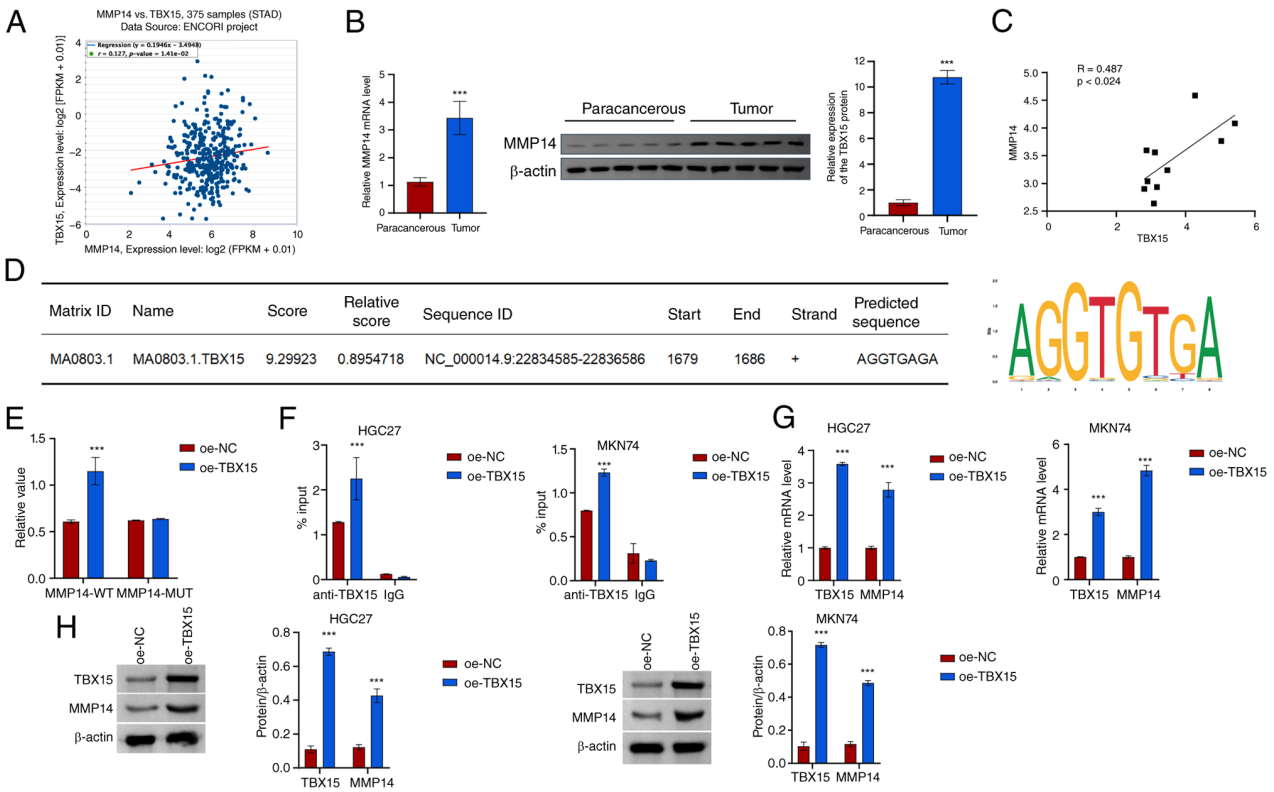

Figure 4. Transcription factor TBX15 targeted the *MMP14* promoter. (A) Correlation analysis between *TBX15* and *MMP14* (n=375). (B) MMP14 expression. ***P<0.001 vs. paracancerous, two-tailed t-test. (C) Pearson correlation analysis. (D) Binding sites between transcription factor TBX15 and *MMP14* promoter and the matrix for TBX15 binding. (E) The *MMP14* promoter activity was validated. (F) ChIP-PCR analysis. (G) Levels of *TBX15* and *MMP14* mRNA. (H) Protein expression of TBX15 and MMP14. ***P<0.001 vs. oe-NC, two-way ANOVA. TBX15, T-box transcription factor 15; MMP14, matrix metalloproteinase 14; oe-, overexpression; NC, negative control.

the expression of *TBX15* and *MMP14* was predicted to be positively correlated (Fig. 4A). *MMP14* mRNA and protein levels increased in GC tissues, and *TBX15* was positively correlated with *MMP14* (Fig. 4B and C). JASPAR online prediction found that the transcription factor TBX15 might target the *MMP14* promoter (Fig. 4D). A dual luciferase reporter gene was used to verify the activity of the *MMP14* promoter. Overexpression of *TBX15* increased *MMP14* promoter activity (Fig. 4E). ChIP-PCR assay showed that TBX15 interacted with the *MMP14* promoter (Fig. 4F). Overexpression of *TBX15* was found to promote *MMP14* mRNA and protein expression (Fig. 4G and H). These results suggested that the transcription factor TBX15 may target the *MMP14* promoter to regulate its transcriptional activity.

Knockdown of TBX15 inhibits the immune evasion of GC cells. The relationship between TBX15 and immune cells was further explored. In the GC microenvironment, macrophages were enriched, while $CD8^+$ T cell infiltration level was significantly reduced (43). Macrophages play a crucial role in the innate immune system. Under different microenvironmental stimuli, macrophages can transform into two different subtypes (M1 and M2), which have completely different molecular phenotypes and functional characteristics. TAMs are macrophages that differentiate under the influence of various factors in the tumor microenvironment (TME) and have the characteristics and functions of M2-type macrophages. To analyze the role of TBX15 and MMP14 in GC immune escape, a co-culture system of GC cells and macrophages was constructed. After intervention with *TBX15* silencing and *MMP14* overexpression, GC cells were then co-cultured with macrophages (Fig. 5A; Fig. S3A and B). *TBX15* silencing promoted the levels of M1-type TAM cells and decreased the M2-type levels (Fig. 5B and C; Fig. S3C and D). The gating strategy of Fig. S4A and B was used to gate the cell subsets. M1 macrophage markers (*iNOS*, *IL-1β* and *TNF-α*) were increased after *TBX15* silencing, and the opposite was observed for M2 macrophage markers (*Arg-1*, *IL-10* and *CD206*) (Fig. 5D and E; Fig. S3E and F). These results suggested that *TBX15* silencing promotes TAMs toward an M1 proinflammatory phenotype. Overexpression of *MMP14* decreased the levels of *iNOS*, *IL-1β* and *TNF-α* and increased *Arg-1*, *IL-10* and *CD206*. This indicated that overexpression of *MMP14* reduced the regulatory effect of *TBX15* silencing on macrophage polarization.

In addition, $CD8^+$ T cell-associated cytokines GZMB, PFP, CD100, IFN-γ and TNF-α were identified in the co-culture system constructed by MFC cells and $CD8^+$ T cells. In the *TBX15*-silenced co-culture system, GZMB, PFP, CD100, IFN-γ and TNF-α levels increased. Silencing *TBX15* enhanced $CD8^+$ T cell activation and antitumor immunity. Overexpression of *MMP14* reduced the levels of GZMB, PFP, CD100, IFN-γ, and TNF-α (Fig. 5F and G).

In summary, TBX15 participates in the immune escape process of GC by promoting macrophage M2 polarization and inhibiting $CD8^+$ T cell activation.

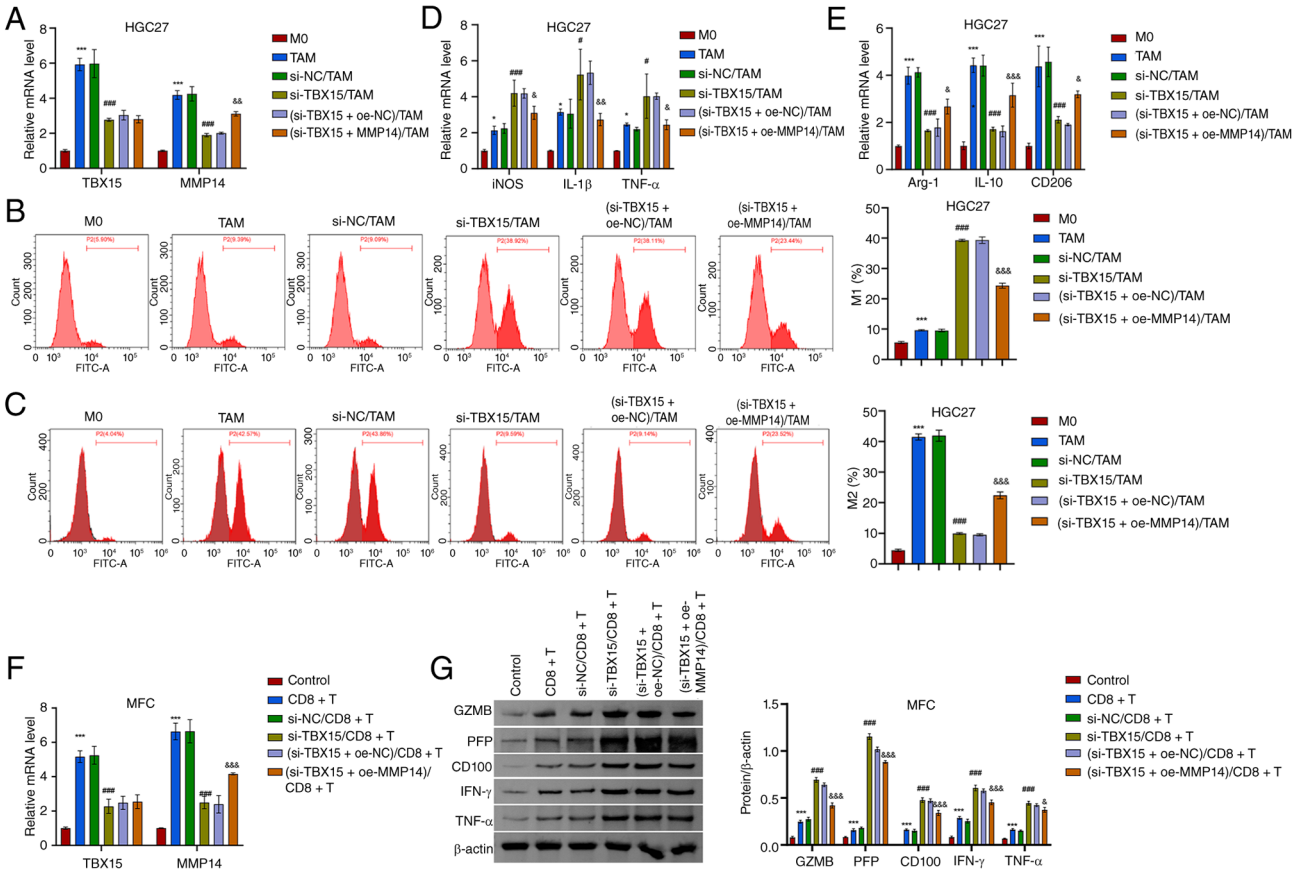

Figure 5. TBX15 and MMP14 participate in macrophage polarization and CD8$^+$ T cell processes. (A) *TBX15* and *MMP14* mRNA levels in HGC27 cells. (B and C) Percentage of M1- and M2-type macrophages in the co-culture system of GC cell-TAMs. (D and E) Expression of *iNOS*, *IL-1β*, *TNF-α*, *Arg-1*, *IL-10* and *CD206*. *P<0.05 and ***P<0.001 vs. M0; $^{\#}$P<0.05 and $^{\#\#\#}$P<0.001 vs. si-NC/TAM; $^{\&}$P<0.05, $^{\&\&}$P<0.01 and $^{\&\&\&}$P<0.001 vs. (si-*TBX15* + oe-NC)/TAM, one-way ANOVA and two-way ANOVA. (F) *TBX15* and *MMP14* mRNA levels in MFC. (G) Expression of GZMB, PFP, CD100, IFN-γ and TNF-α in the co-culture system of MFC cell-CD8$^+$ T cells. ***P<0.001 vs. control; $^{\#\#\#}$P<0.001 vs. si-NC/CD8$^+$ T; $^{\&}$P<0.05 and $^{\&\&\&}$P<0.001 vs. (si-*TBX15* + oe-NC)/CD8$^+$ T, two-way ANOVA. TBX15, T-box transcription factor 15; MMP14, matrix metalloproteinase 14; TAMs, tumor-associated macrophages; iNOS, inducible nitric oxide synthase; oe-, overexpression; NC, negative control; si-, small interfering; MFC, mouse forestomach carcinoma; GZMB, granzyme B; PFP, perforin.

METTL3 mediates m6A modification of TBX15. The SRAMP online website predicted that *TBX15* might undergo m6A modification, and RM2Target predicted that *TBX15* would bind to the m6A methyltransferase METTL3 (Fig. S5A and B). In GC, METTL3 expression and total m6A levels were increased (Fig. 6A-C). METTL3 expression and total m6A level increased in HGC27 (*METTL3* mRNA: 4.02±0.34; METTL3: 0.44±0.03; m6A%: 0.12±0.01) and MKN74 (*METTL3* mRNA: 3.68±0.38; METTL3: 0.48±0.02; m6A%: 0.12±0.01) compared with GES-1 (*METTL3* mRNA: 1.00±0.11; METTL3: 0.04±0; m6A%: 0.07±0.02) (Fig. 6D-F). To further explore the regulatory relationship between METTL3 and *TBX15*, *METTL3* silenced cells were constructed (Figs. 6G and S5C). After silencing *METTL3*, the m6A level of *TBX15* was decreased (Figs. 6H and S5D). Results proved that METTL3 binds to *TBX15* mRNA (Figs. 6I and S5E). *METTL3* silencing reduced *TBX15* mRNA stability (Figs. 6J and S5F). These results indicated that silencing METTL3 inhibits the m6A level of *TBX15* and reduces *TBX15* mRNA stability.

METTL3/TBX15/MMP14 signaling axis regulates proliferation, migration ability and immune escape process in GC. To explore whether METTL3 regulates GC cell function and development through the TBX15/MMP14 signaling axis, *METTL3* silencing and *TBX15* overexpression cells were constructed. *METTL3* silencing inhibited MMP14 expression, and *TBX15* overexpression attenuated the inhibitory effect of *METTL3* silencing on MMP14 expression (Figs. 7A and S6A). *METTL3* silencing decreased proliferation activity and increased apoptotic rate of GC cells (Fig. 7B-D; Fig. S6B-D). Overexpression of *TBX15* increased proliferation and decreased apoptosis. Overexpression of *TBX15* reduced the inhibitory effect of *METTL3* silencing on migration (Figs. 7E and S6E). Under the intervention conditions of *METTL3* silencing and *TBX15* overexpression, cell invasion was altered, consistent with migration (Figs. 7F and S6F).

Next, the role of METTL3/TBX15/MMP14 signaling axis in GC cell immune escape was further analyzed. Silencing *METTL3* promoted the polarization of TAMs to M1 macrophages in the co-culture system of GC cell-macrophages (Fig. 7G and H; Fig. S6G and H; Fig. S7A and B). Levels of *iNOS*, *IL-1β* and *TNF-α* increased, and *Arg-1*, *IL-10* and *CD206* decreased (Fig. 7I and J; Fig. S6I and J). Overexpression of *TBX15* reduced the effect of *METTL3* silencing. In the co-culture system of MFC cell-CD8$^+$ T cells, the expression of GZMB, PFP, CD100, IFN-γ and TNF-α increased after *METTL3* silencing. Overexpression of *TBX15* inhibited the regulation of *METTL3* silencing on CD8$^+$ T cell-related cytokines GZMB,

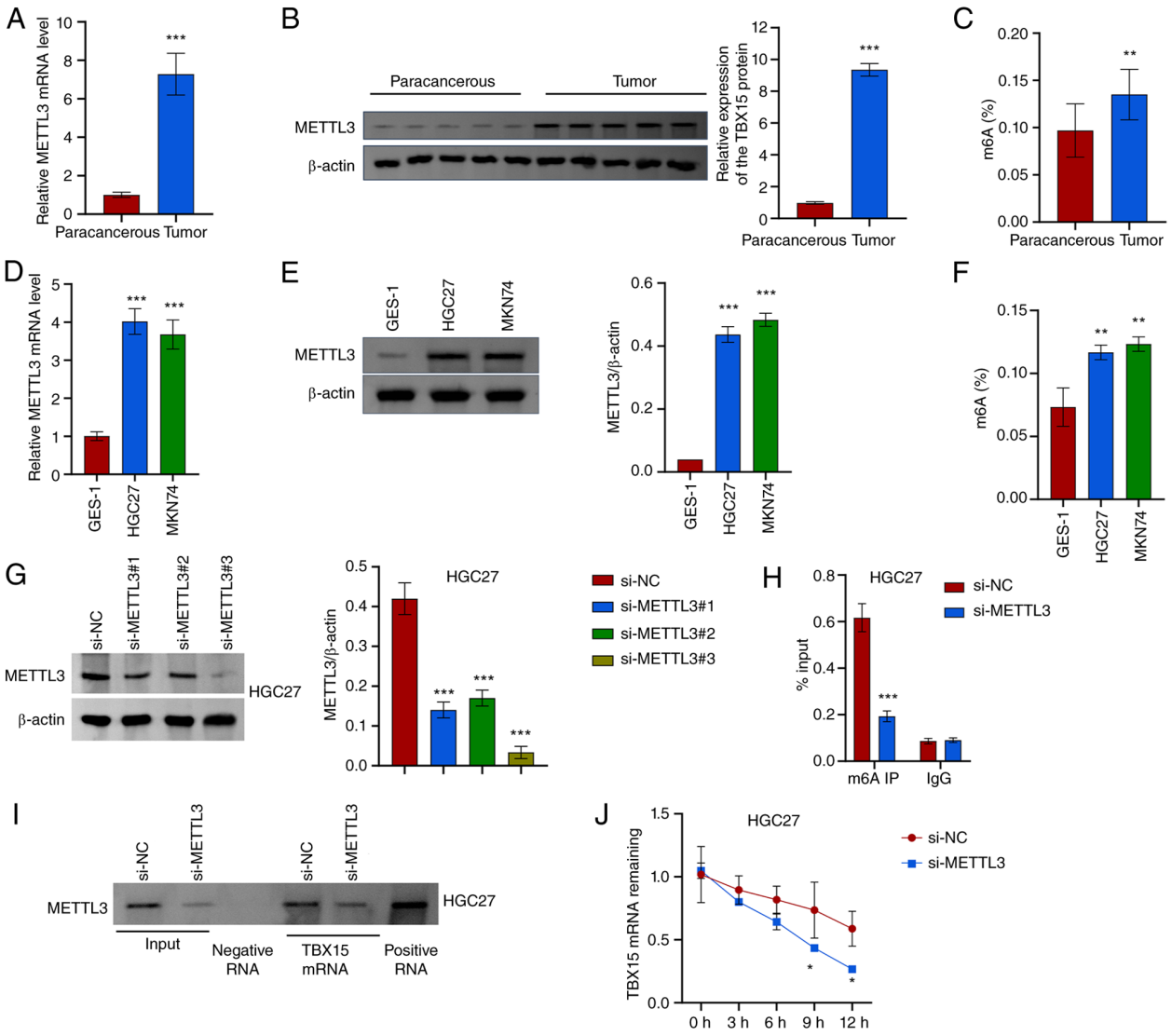

Figure 6. Silencing *METTL3* inhibits the m6A level of *TBX15*. (A and B) Levels of METTL3 in GC tissues. (C) Total m6A methylation level. **P<0.01 and ***P<0.001 vs. paracancerous, two-tailed t-test. (D and E) Expression of METTL3 in HGC27. (F) Total m6A methylation level. **P<0.01 and ***P<0.001 vs. GSE-1, one-way ANOVA. (G) METTL3 levels were detected after silencing *METTL3* in HGC27. (H) The m6A level of *TBX15*. (I) RNA Pull-down assay. (J) The stability of *TBX15* mRNA. *P<0.05 and ***P<0.001 vs. si-NC, one-way ANOVA and two-way ANOVA. METTL3, methyltransferase-like 3; m6A, N6-methyladenosine; TBX15, T-box transcription factor 15; NC, negative control; si-, small interfering; GC, gastric cancer.

PFP, CD100, IFN-γ and TNF-α (Fig. 7K). METTL3 regulated proliferation, migratory activity and immune escape process through TBX15/MMP14 signaling axis in GC.

METTL3 regulates the tumorigenic ability of MFC cells in mice through TBX15/MMP14 axis. The effect of METTL3/TBX15/MMP14 signaling axis on MFC cells' ability to induce tumorigenesis in mice was further analyzed. MFC cells with *METTL3* silencing and *TBX15* overexpression were injected subcutaneously into mice. After 21 days, tumor volume and weight were reduced after *METTL3* silencing. Overexpression of *TBX15* attenuated the effect of *METTL3* silencing, and the tumor weight and volume (maximum diameter: 14.99 mm, maximum volume: 1,385.54 mm^3) increased (Fig. 8A-C). Levels of METTL3, TBX15 and MMP14 were reduced after *METTL3* silencing. Overexpression of *TBX15* promoted TBX15 and MMP14 levels but had no significant regulatory effect on METTL3 (Fig. 8D and E). In the tumor, the apoptotic rate increased and the expression of Ki67 decreased after *METTL3* silencing. Overexpression of *TBX15* decreased the apoptotic rate and increased the expression of Ki67 (Fig. 8F and G). Similarly, the expression of M1 macrophage markers (iNOS, IL-1β and TNF-α) was increased after *METTL3* silencing, and overexpression of *TBX15* reduced the effect of *METTL3* silencing. Levels of M2 macrophage markers (Arg-1, IL-10 and CD206) were opposite (Fig. 8H). Overexpression of *TBX15* inhibited the regulation of *METTL3* silencing on $CD8^+$ T cell-related cytokines GZMB, PFP, CD100, IFN-γ and TNF-α (Figs. 8I and S8). The aforementioned results suggested that silencing *METTL3* inhibits tumor development, via the TBX15/MMP14 signaling axis.

Discussion

The experimental design of the present study is shown in Fig. S5. It is suggested that high expression of TBX15 in

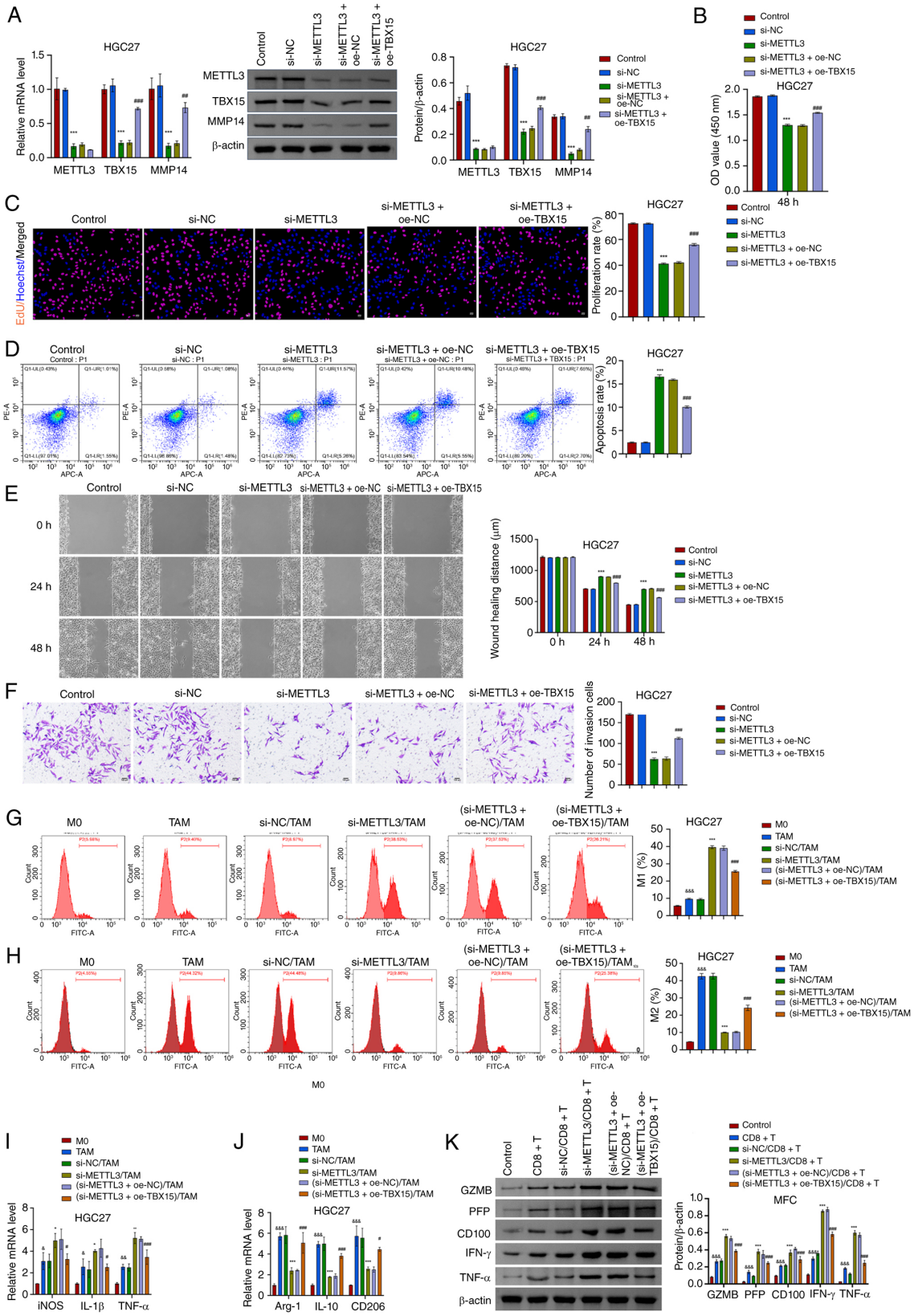

Figure 7. METTL3 regulates GC cell function and development through the TBX15/MMP14 signaling axis. (A) The expression of METTL3, TBX15 and MMP14 was identified after *METTL3* silencing and *TBX15* overexpression. (B and C) Analysis of GC cell proliferation activity. Scale bar, 50 μm. (D) Flow cytometric analysis of GC cell apoptosis. (E and F) Migration and invasion assays. Scale bar, 100 μm. ***P<0.001 vs. si-NC; $^{\#\#}$P<0.01 and $^{\#\#\#}$P<0.001 vs. si-*METTL3* + oe-NC, one-way ANOVA and two-way ANOVA. (G and H) In the co-culture system of GC cell-macrophages, the proportion of M1 and M2 macrophages was analyzed after *METTL3* silencing and *TBX15* overexpression intervention. (I and J) Levels of *iNOS*, *IL-1β*, *TNF-α*, *Arg-1*, *IL-10* and *CD206*. $^{\&}$P<0.05, $^{\&\&}$P<0.01 and $^{\&\&\&}$P<0.001 vs. M0; *P<0.05, **P<0.01 and ***P<0.001 vs si-NC/TAM; $^{\#}$P<0.05 and $^{\#\#\#}$P<0.001 vs. (si-*METTL3* + oe-NC)/TAM, one-way ANOVA and two-way ANOVA. (K) Levels of CD8^{+} T cell-related cytokines (GZMB, PFP, CD100, IFN-γ and TNF-α) expression after intervention of *METTL3* silencing and *TBX15* overexpression. $^{\&\&\&}$P<0.001 vs. control, ***P<0.001 vs. si-NC/CD8^{+} T and $^{\#\#\#}$P<0.001 vs. (si-*METTL3* + oe-NC)/CD8^{+} T, two-way ANOVA. METTL3, methyltransferase-like 3; GC, gastric cancer; TBX15, T-box transcription factor 15; MMP14, matrix metalloproteinase 14; NC, negative control; si-, small interfering; oe-, overexpression; GZMB, granzyme B; PFP, perforin.

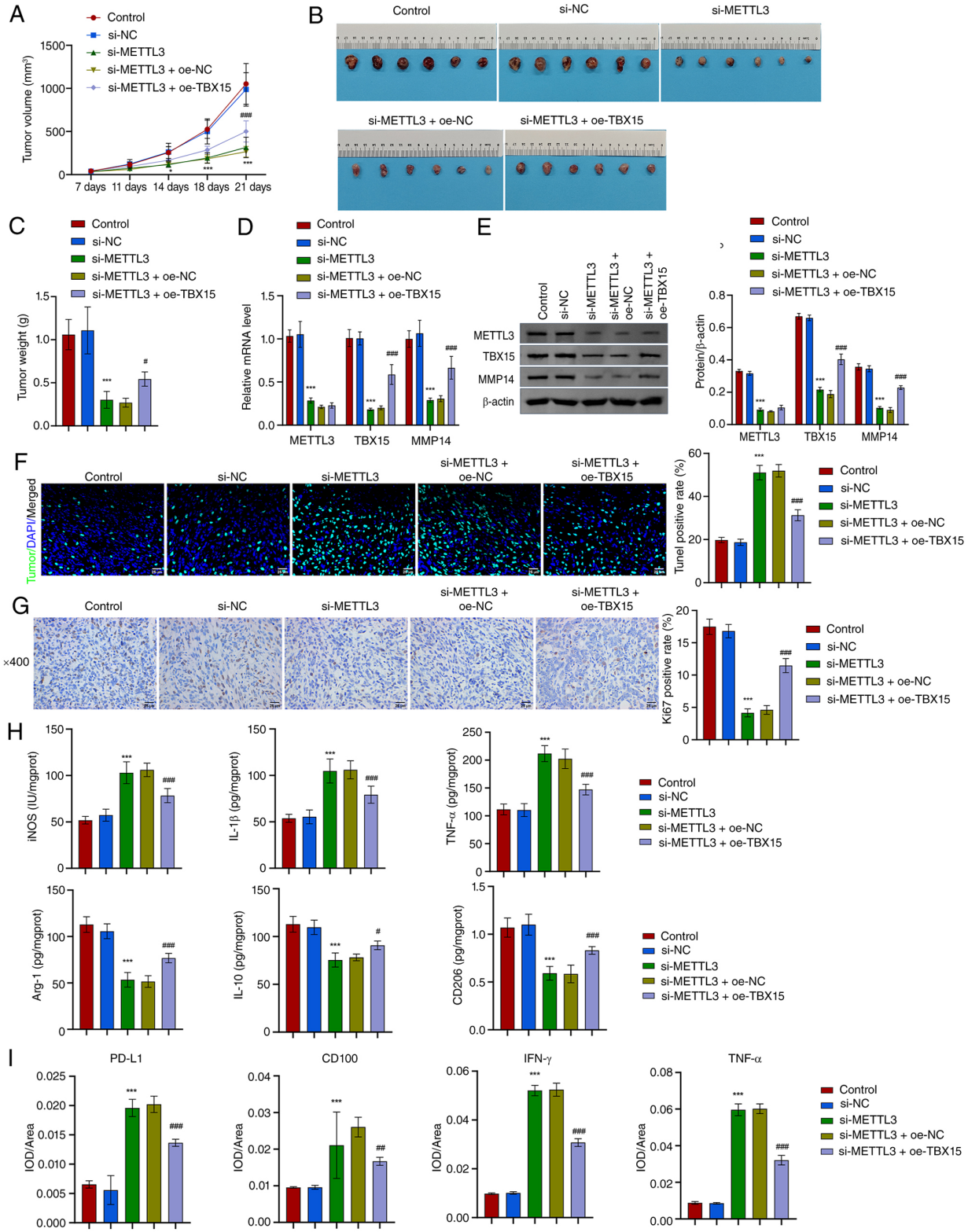

Figure 8. *In vivo* experimental validation of the METTL3/TBX15/MMP14 axis. (A) Tumor growth curve. (B) Images of the tumor. (C) Tumor weight. (D and E) METTL3, TBX15 and MMP14 levels in tumors. (F) TUNEL analysis. Scale bar, 25 μm. (G) Ki67 expression via immunohistochemical analysis. Scale bar, 25 μm. (H) Levels of iNOS, IL-1β, TNF-α, Arg-1, IL-10 and CD206. (I) PD-L1, CD100, IFN-γ and TNF-α expression via immunohistochemical analysis. *P<0.05 and ***P<0.001 vs. sh-NC; $^{\#}$P<0.05, $^{\#\#}$P<0.01 and $^{\#\#\#}$P<0.001 vs. sh-*METTL3* + oe-NC, one-way ANOVA and two-way ANOVA. METTL3, methyltransferase-like 3; TBX15, T-box transcription factor 15; MMP14, matrix metalloproteinase 14; iNOS, inducible nitric oxide synthase; PD-L1, programmed death-ligand 1; IFN, interferon; NC, negative control; oe-, overexpression; sh-, short hairpin.

GC was linked to shorter survival of patients. Suppression of *TBX15* led to elevated levels of apoptosis and hindered the proliferation and invasion of GC cells. Consistent with a previous study, *TBX15* silencing stimulated increased apoptosis in cancer cells (44), and high levels of *TBX15* predicted poor prognosis in patients with cancer (19). This evidence suggested

that *TBX15* is regulated by m6A methylation modification and interacts with the m6A methyltransferase METTL3. In a GC study, METTL3 was associated with tumor malignant progression and poor prognosis of patients (37). Silencing *METTL3* reduced *TBX15* mRNA stability. Overexpression of *TBX15* reduced the inhibitory effect of *METTL3* silencing on GC cell proliferation and invasion to a certain extent. Meanwhile, TBX15 could regulate the transcription of *MMP14* by targeting its promoter. In GC, MMP14 is a target enzyme used to detect GC peritoneal metastasis (45), and its high expression predicts poor prognosis of patients with GC (46). As one of the membrane-type matrix metalloproteinases, MMP14 plays an important role in tumor development and metastasis by promoting the decomposition of cell adhesion molecules, destroying the basement membrane and destroying the extracellular matrix (47,48). Therefore, it is reasonable to hypothesize that *TBX15* regulated by m6A methylation modification may have the involvement of MMP14 in controlling the migration and invasion process of GC cells.

In addition, overexpression of *TBX15* reduced glycolysis, glucose uptake and lactate production in GC cells (21). The 'glycolytic switch', also known as the 'Warburg effect', can lead to the accumulation of lactate and lactate in the tumor environment, thereby promoting tumor immune escape (49). Overexpression of *MMP14* reversed the inhibitory effect of *TBX15* silencing on M2 macrophage polarization and the promoting effect on M1 macrophages in the GC cell-TAM cell co-culture system. M2 macrophages are important tumor supporting cells in tumor development and promote the immune escape of tumor cells by regulating the immune checkpoints (50,51). MMP14 was involved in the polarization of M2 macrophages (52). Blockade of MMP14 increases iNOS and polarizes macrophages to an antitumor phenotype (53). This further confirms the findings that TBX15, an intracellular transcription factor, regulates macrophage to tumor-promoting phenotypic polarization by targeting *MMP14*, thereby promoting cancer development. On the other hand, $CD8^+$ T cells can participate in antitumor immunity by secreting inflammatory cytokines (IFN-γ and TNF-α) and cytotoxic factors (GZMB and PFP) (54). In the MFC cell-$CD8^+$ T cell co-culture system, overexpression of *MMP14* inhibited the expression of antitumor related cytokines of $CD8^+$ T cells, including GZMB, PFP, IFN-γ and TNF-α. As effective effector cells in the TME, $CD8^+$ T cells can induce tumor cell apoptosis by secreting cytotoxic factors (GZMB and PFP). In the tumor immune microenvironment, cells with high levels of MMP14 can transport tsRNA through exosomes and inhibit the activity of $CD8^+$ T cells (55). MMP14 promotes the shedding of membrane-bound CD100 (mCD100) from the membrane of $CD8^+$ T cells, thereby promoting the elevation of $CD8^+$ T cell response (56). Thus, the TBX15/MMP14 signaling axis promotes tumor development and cancer cell immune escape in GC cells, possibly by promoting M2 macrophage polarization and inhibiting $CD8^+$ T cell antitumor activity. In the future, the regulatory mechanism of MMP14 in immune escape of GC cells will be further refined.

It should be pointed out that the present study did not investigate whether m6A readers are involved in TBX15 mRNA stability or translational regulation. Considering that METTL3 mainly plays the function of m6A 'writer', the transmission of its regulatory effect is often dependent on the downstream mediation of the m6A readers. Therefore, the current study has not fully revealed the regulatory pathway of 'METTL3-m6A-Reader-TBX15', which is the main limitation and the direction of future research needs to be focused on improving. In future studies, it is planned to collect clinical samples and analyze the correlation between m6A readers and TBX15 based on clinical samples and further explore its internal regulatory pathways by RIP-qPCR and co-expression analysis of m6A readers. The authors acknowledge that although the clinical sample (n=10) provided preliminary evidence, it was insufficient to ensure statistical generalizability, and potential selection bias (for example from a single institution) cannot be ruled out. Validation in a larger multicenter cohort is needed. Limited to a single subcutaneous model may not fully recapitulate the heterogeneous human GC immune microenvironment, particularly immune cell composition and cytokine signaling. This is also one of the limitations of the present study. It would be helpful to construct an orthotopic tumor model to verify the role of target genes in tumor development in numerous ways. Alternatively, it is noted that the immortalized cell lines lack a patient-specific genetic background. Future studies using primary cells are needed. Other potential biases, including the lack of clinical follow-up and survival data, are a limitation of the present study. Continuing to collect patient follow-up and survival information is the authors' next arrangement.

The results of the present study demonstrated that the m6A modification of TBX15 is regulated by the m6A methyltransferase METTL3. TBX15 regulates GC cell proliferation, migration and invasion through MMP14. The METTL3/TBX15/MMP14 signaling axis promotes the polarization of macrophages to M2 and inhibits the antitumor activity of $CD8^+$ T cells. The results of the present study suggested that TBX15 is involved in the process of proliferation, migration and invasion of GC cells. Combined with the results of GC cell-TAM cells and MFC cell-$CD8^+$ T cell co-culture systems, it is suggested that TBX15 is connected with the polarization of macrophages in the TME and the antitumor activity of $CD8^+$ T cells. This suggested that TBX15 may be a promising target for alleviating immunosuppression.

Acknowledgements

Not applicable.

Funding

The present study was supported by the Natural Science Foundation of Hunan (grant nos. 2021JJ70076, 2023JJ50217, 2025JJ70002 and 2022JJ50104).

Availability of data and materials

The data generated in the present study are included in the figures and/or tables of this article. The data generated in the present study may be requested from the corresponding author.

Authors' contributions

WQ and HH conceptualized the study, acquired funding and resources, and wrote, reviewed and edited the manuscript. HH,

RH, ML, XL, QA, MC, QW, WC and WQ curated data. HH conducted rmal analysis, developed methodology, performed data validation and visualization, and wrote the original draft. HH, RH, ML, XL and MC conducted investigation. WQ conducted project administration and supervised the study. All authors read and approved the final version of the manuscript. WQ and HS confirm the authenticity of all the raw data.

Ethics approval and consent to participate

The procedures followed in the present study were approved (approval no. ZZCHEC2022070-01) by the Ethics Committee of Zhuzhou Central Hospital (Zhuzhou Hospital Affiliated to Xiangya School of Medicine, Central South University; Zhuzhou, China). Written informed consent was obtained from each enrolled subject. All animal experiments were performed in accordance with the relevant guidelines and regulations and were approved by Animal Ethical and Welfare Committee of The Second Xiangya Hospital (approval no. 2022722; Zhuzhou, China).

Patient consent for publication

Not applicable.

Competing interests

The authors declare that they have no competing interests.

References

1. Qiu H, Cao S and Xu R: Cancer incidence, mortality, and burden in China: A time-trend analysis and comparison with the United States and United Kingdom based on the global epidemiological data released in 2020. Cancer Commun (Lond) 41: 1037-1048, 2021.
2. Tan P and Yeoh KG: Genetics and molecular pathogenesis of gastric adenocarcinoma. Gastroenterology 149: 1153-1162.e3, 2015.
3. Zhang M, Zhong A, Liu H, Zhao L, Wang Y, Lu Z, Zhang L, Pan X, Liang Z, Gao L, *et al*: EZH2 loss promotes gastric squamous cell carcinoma. Nat Commun 16: 6032, 2025.
4. Tao B, Wang Z, Wang X, Song A, Liu J, Wang J, Zhang Q, Chen Z, Wang Z, Xu W, *et al*: An inherited predisposition allele promotes gastric cancer via enhancing deubiquitination-mediated activation of epithelial-to-mesenchymal transition signaling. J Clin Invest 135: e179617, 2025.
5. Cancer Genome Atlas Research Network: Comprehensive molecular characterization of gastric adenocarcinoma. Nature 513: 202-209, 2014.
6. Keller G, Grimm V, Vogelsang H, Bischoff P, Mueller J, Siewert JR and Höfler H: Analysis for microsatellite instability and mutations of the DNA mismatch repair gene hMLH1 in familial gastric cancer. Int J Cancer 68: 571-576, 1996.
7. Richards FM, McKee SA, Rajpar MH, Cole TR, Evans DG, Jankowski JA, McKeown C, Sanders DS and Maher ER: Germline E-cadherin gene (CDH1) mutations predispose to familial gastric cancer and colorectal cancer. Hum Mol Genet 8: 607-610, 1999.
8. Lu L, Mullins CS, Schafmayer C, Zeißig S and Linnebacher M: A global assessment of recent trends in gastrointestinal cancer and lifestyle-associated risk factors. Cancer Commun (Lond) 41: 1137-1151, 2021.
9. Ajani JA, Lee J, Sano T, Janjigian YY, Fan D and Song S: Gastric adenocarcinoma. Nat Rev Dis Primers 3: 17036, 2017.
10. Matsuoka T and Yashiro M: Bioinformatics analysis and validation of potential markers associated with prediction and prognosis of gastric cancer. Int J Mol Sci 25: 5880, 2024.
11. Guan WL, He Y and Xu RH: Gastric cancer treatment: Recent progress and future perspectives. J Hematol Oncol 16: 57, 2023.
12. Farin HF, Bussen M, Schmidt MK, Singh MK, Schuster-Gossler K and Kispert A: Transcriptional repression by the T-box proteins Tbx18 and Tbx15 depends on Groucho corepressors. J Biol Chem 282: 25748-25759, 2007.
13. Kispert A and Herrmann BG: The Brachyury gene encodes a novel DNA binding protein. Embo J 12: 3211-3220, 1993.
14. Ahmed A, Syed JN, Chi L, Wang Y, Perez-Romero C, Lee D, Kocaqi E, Caballero A, Yang J, Escalante-Covarrubias Q, *et al*: KDM8 epigenetically controls cardiac metabolism to prevent initiation of dilated cardiomyopathy. Nat Cardiovasc Res 2: 174-191, 2023.
15. Ye W, Wang Y, Hou S, Mei B, Liu X, Huang H, Zhou Q, Niu Y, Chen Y, Zhang M and Huang Q: USF3 modulates osteoporosis risk by targeting WNT16, RANKL, RUNX2, and two GWAS lead SNPs rs2908007 and rs4531631. Hum Mutat 42: 37-49, 2021.
16. Pan DZ, Miao Z, Comenho C, Rajkumar S, Koka A, Lee SHT, Alvarez M, Kaminska D, Ko A, Sinsheimer JS, *et al*: Identification of TBX15 as an adipose master trans regulator of abdominal obesity genes. Genome Med 13: 123, 2021.
17. Li P, Li Y, Bai S, Zhang Y and Zhao L: miR-4732-3p prevents lung cancer progression via inhibition of the TBX15/TNFSF11 axis. Epigenomics 15: 195-207, 2023.
18. Ge Y, Jia B, Zhang P, Chen B, Liu L, Shi Y, Huang S, Liu X, Wang R, Xie Y, *et al*: TBX15 facilitates malignant progression of glioma by transcriptional activation of TXDNC5. iScience 27: 108950, 2024.
19. Yan D, Yu Y, Ni Q, Meng Q, Wu H, Ding S, Liu X, Tang C, Liu Q and Yang K: The overexpression and clinical significance of TBX15 in human gliomas. Sci Rep 13: 9771, 2023.
20. Golozar M, Motlagh AV, Mahdevar M, Peymani M, InanlooRahatloo K and Ghaedi K: TBX15 and SDHB expression changes in colorectal cancer serve as potential prognostic biomarkers. Exp Mol Pathol 136: 104890, 2024.
21. Gu P and Wu LN: Sulforaphane targets the TBX15/KIF2C pathway to repress glycolysis and cell proliferation in gastric carcinoma cells. Nutr Cancer 75: 1263-1270, 2023.
22. Wei G: RNA m6A modification, signals for degradation or stabilisation? Biochem Soc Trans 52: 707-717, 2024.
23. Hu Y, Gong C, Li Z, Liu J, Chen Y, Huang Y, Luo Q, Wang S, Hou Y, Yang S and Xiao Y: Demethylase ALKBH5 suppresses invasion of gastric cancer via PKMYT1 m6A modification. Mol Cancer 21: 34, 2022.
24. Shu F, Liu H, Chen X, Liu Y, Zhou J, Tang L, Cao W, Yang S, Long Y, Li R, *et al*: m6A modification promotes EMT and metastasis of castration-resistant prostate cancer by upregulating NFIB. Cancer Res 84: 1947-1962, 2024.
25. Wang J, Zhang J, Liu H, Meng L, Gao X, Zhao Y, Wang C, Gao X, Fan A, Cao T, *et al*: N6-methyladenosine reader hnRNPA2B1 recognizes and stabilizes NEAT1 to confer chemoresistance in gastric cancer. Cancer Commun (Lond) 44: 469-490, 2024.
26. Jin T, Yang L, Chang C, Luo H, Wang R, Gan Y, Sun Y, Guo Y, Tang R, Chen S, *et al*: HnRNPA2B1 ISGylation regulates m6A-Tagged mRNA selective export via ALYREF/NXF1 complex to foster breast cancer development. Adv Sci (Weinh) 11: e2307639, 2024.
27. Qiao Y, Sun Q, Chen X, He L, Wang D, Su R, Xue Y, Sun H and Wang H: Nuclear m6A reader YTHDC1 promotes muscle stem cell activation/proliferation by regulating mRNA splicing and nuclear export. Elife 12: e82703, 2023.
28. Alarcón CR, Goodarzi H, Lee H, Liu X, Tavazoie S and Tavazoie SF: HNRNPA2B1 is a mediator of m(6)A-dependent nuclear RNA processing events. Cell 162: 1299-1308, 2015.
29. Wang X, Lu Z, Gomez A, Hon GC, Yue Y, Han D, Fu Y, Parisien M, Dai Q, Jia G, *et al*: N6-methyladenosine-dependent regulation of messenger RNA stability. Nature 505: 117-120, 2014.
30. Bokar JA, Shambaugh ME, Polayes D, Matera AG and Rottman FM: Purification and cDNA cloning of the AdoMet-binding subunit of the human mRNA (N6-adenosine)-methyltransferase. RNA 3: 1233-1247, 1997.
31. Zaccara S, Ries RJ and Jaffrey SR: Reading, writing and erasing mRNA methylation. Nat Rev Mol Cell Biol 20: 608-624, 2019.
32. Zeng Y, Luo Y, Zhao K, Liu SS, Wu KK, Wu YY, Du KK, Pan W, Dai Y, Liu Y, *et al*: m6A-mediated induction of 7-dehydrocholesterol reductase stimulates cholesterol synthesis and cAMP signaling to promote bladder cancer metastasis. Cancer Res 84: 3402-3418, 2024.
33. Wang J, Fan P, Shen P, Fan C, Zhao P, Shen Y, Dong K, Ling R, Chen S and Zhang J: XBP1s activates METTL3/METTL14 for ER-phagy and paclitaxel sensitivity regulation in breast cancer. Cancer Lett 596: 216846, 2024.

34. Li T, Hu PS, Zuo Z, Lin JF, Li X, Wu Q, Chen ZH, Zeng ZL, Wang F, Zheng J, *et al*: METTL3 facilitates tumor progression via an m(6)A-IGF2BP2-dependent mechanism in colorectal carcinoma. Mol Cancer 18: 112, 2019.
35. Wang Q, Guo X, Li L, Gao Z, Su X, Ji M and Liu J: N(6)-methyladenosine METTL3 promotes cervical cancer tumorigenesis and Warburg effect through YTHDF1/HK2 modification. Cell Death Dis 11: 911, 2020.
36. Wang J, Yu H, Dong W, Zhang C, Hu M, Ma W, Jiang X, Li H, Yang P and Xiang D: N6-Methyladenosine-Mediated Up-Regulation of FZD10 regulates liver cancer stem cells' properties and lenvatinib resistance through WNT/β-catenin and hippo signaling pathways. Gastroenterology 164: 990-1005, 2023.
37. Wei X, Huo Y, Pi J, Gao Y, Rao S, He M, Wei Q, Song P, Chen Y, Lu D, *et al*: METTL3 preferentially enhances non-m(6)A translation of epigenetic factors and promotes tumourigenesis. NaT cell Biol 24: 1278-1290, 2022.
38. Xu X, Li Y, Wu Y, Wang M, Lu Y, Fang Z, Wang H and Li Y: Increased ATF2 expression predicts poor prognosis and inhibits sorafenib-induced ferroptosis in gastric cancer. Redox Biol 59: 102564, 2023.
39. Livak KJ and Schmittgen TD: Analysis of relative gene expression data using real-time quantitative PCR and the 2(-Delta Delta C(T)) method. Methods 25: 402-408, 2001
40. He Z, Jiao H, An Q, Zhang X, Zengyangzong D, Xu J, Liu H, Ma L and Zhao W: Discovery of novel 4-phenylquinazoline-based BRD4 inhibitors for cardiac fibrosis. Acta Pharm Sin B 12: 291-307, 2022.
41. Zheng Z, Lin F, Zhao B, Chen G, Wei G, Chen X, Nie R, Zhang R, Zhao Z, Zhou Z, *et al*: ALKBH5 suppresses gastric cancer tumorigenesis and metastasis by inhibiting the translation of uncapped WRAP53 RNA isoforms in an m6A-dependent manner. Mol Cancer 24: 19, 2025.
42. Wei J, Yin Y, Zhou J, Chen H, Peng J, Yang J and Tang Y: METTL3 potentiates resistance to cisplatin through m(6) A modification of TFAP2C in seminoma. J Cell Mol Med 24: 11366-11380, 2020.
43. Thorsson V, Gibbs DL, Brown SD, Wolf D, Bortone DS, Yang TH, Porta-Pardo E, Gao GF, Plaisier CL, Eddy JA, *et al*: The immune landscape of cancer. Immunity 48: 812-830.e814, 2018.
44. Arribas J, Giménez E, Marcos R and Velázquez A: Novel anti-apoptotic effect of TBX15: overexpression of TBX15 reduces apoptosis in cancer cells. Apoptosis 20: 1338-1346, 2015.
45. Ogawa S, Kubo H, Murayama Y, Kubota T, Yubakami M, Matsumoto T, Ohashi T, Okamoto K, Kuriki Y, Hanaoka K, *et al*: Matrix metalloprotease-14 is a target enzyme for detecting peritoneal metastasis in gastric cancer. Photodiagnosis Photodyn Ther 35: 102420, 2021.
46. Kasurinen A, Gramolelli S, Hagström J, Laitinen A, Kokkola A, Miki Y, Lehti K, Yashiro M, Ojala PM, Böckelman C and Haglund C: High tissue MMP14 expression predicts worse survival in gastric cancer, particularly with a low PROX1. Cancer Med 8: 6995-7005, 2019.
47. Chen WC, Chang AC, Tsai HC, Liu PI, Huang CL, Guo JH, Liu CL, Liu JF, Thuong LHH and Tang CH: Bone sialoprotein promotes lung cancer osteolytic bone metastasis via MMP14-dependent mechanisms. Biochem Pharmacol 211: 115540, 2023.
48. Chen M, Qu H, Liang X, Huang Y, Yang Z, Lu P, Shi K, Chen P, Zhang Y, Zhou H, *et al*: Brachyury promotes proliferation and migration of colorectal cancer cells by targeting MMP14. Cancer Cell Int 25: 132, 2025.
49. Siska PJ, Singer K, Evert K, Renner K and Kreutz M: The immunological Warburg effect: Can a metabolic-tumor-stroma score (MeTS) guide cancer immunotherapy? Immunol Rev 295: 187-202, 2020.
50. DeNardo DG, Barreto JB, Andreu P, Vasquez L, Tawfik D, Kolhatkar N and Coussens LM: CD4(+) T cells regulate pulmonary metastasis of mammary carcinomas by enhancing protumor properties of macrophages. Cancer Cell 16: 91-102, 2009.
51. Yang H, Zhang Q, Xu M, Wang L, Chen X, Feng Y, Li Y, Zhang X, Cui W and Jia X: CCL2-CCR2 axis recruits tumor associated macrophages to induce immune evasion through PD-1 signaling in esophageal carcinogenesis. Mol Cancer 19: 41, 2020.
52. Qian J, Li J, Ma H and Ji W: Exosomal circ-ADRM1 promotes lung adenocarcinoma progression and induces macrophage M2 polarization through regulating MMP14 mRNA and protein. Anticancer Drugs 34: 333-343, 2023.
53. Ager EI, Kozin SV, Kirkpatrick ND, Seano G, Kodack DP, Askoxylakis V, Huang Y, Goel S, Snuderl M, Muzikansky A, *et al*: Blockade of MMP14 activity in murine breast carcinomas: Implications for macrophages, vessels, and radiotherapy. J Natl Cancer Inst 107: djv017, 2015.
54. Chen Q, Yin H, Jiang Z, He T, Xie Y, Mao W, Han J, Liu S, Lou W, Wu W, *et al*: Poor clinical outcomes and immunoevasive contexture in $CD161^{+}CD8^{+}$ T cells barren human pancreatic cancer. J Immunother Cancer 12: e008694, 2024.
55. Wang J, Zheng C, Lu J, Xu X, Xiang G, Li J, Zhang J, Mu X and Lu Q: The mechanism of MMP14-positive tumor-associated fibroblast subsets in inhibiting PD-1 immunotherapy for esophageal cancer through exosomal tsRNA-10522. Funct Integr Genomics 24: 186, 2024.
56. Wang HM, Zhang XH, Ye LQ, Zhang K, Yang NN, Geng S, Chen J, Zhao SX, Yang KL and Fan FF: Insufficient CD100 shedding contributes to suppression of CD8(+) T-cell activity in non-small cell lung cancer. Immunology 160: 209-219, 2020.

Copyright © 2026 Hu et al. This work is licensed under a Creative Commons Attribution-NonCommercial-NoDerivatives 4.0 International (CC BY-NC-ND 4.0) License.